Journal of Power Sources 214 (2012) 277–284

Contents lists available at SciVerse ScienceDirect

Journal of Power Sources

journal homepage: www.elsevier.com/locate/jpowsour

Electrodeposition of Pd catalyst layer on graphite rod electrodes for direct formic acid oxidation

Biao Zhang [a,b], Dingding Ye [a,b], Jun Li [a,b], Xun Zhu [a,b,*], Qiang Liao [a,b]

[a] Key Laboratory of Low-grade Energy Utilization Technologies and Systems, Chongqing University, Chongqing 400030, China
[b] Institute of Engineering Thermophysics, Chongqing University, Chongqing 400030, China

HIGHLIGHTS

- A new method for electrodepositing Pd catalyst layer on graphite rods was proposed.
- The Pd catalyst layer showed an island-like morphology and a multi-layer structure.
- Anionic sulfonic groups of Nafion had electrostatic repulsion to $[PdCl_4]^{2-}$ anions.
- Decreased electrodeposition overpotentials led to the formation of Pd islands.
- Predominant Pd (111) made the catalyst highly active toward formic acid oxidation.

ARTICLE INFO

Article history:
Received 27 January 2012
Received in revised form
1 April 2012
Accepted 3 April 2012
Available online 27 April 2012

Keywords:
Palladium catalyst layer
Graphite rod
Electrodeposition
Formic acid electro-oxidation
Microfluidic fuel cell

ABSTRACT

An electrodeposition method for preparing the Pd catalyst layer on graphite rod electrodes for direct formic acid oxidation is proposed in this study. This method consists of a repeated procedure involving the electrodeposition of Pd catalyst onto the graphite rods, followed by Nafion coating (RENC). The structural features and electrocatalytic properties of the electrode were extensively investigated. X-ray diffraction (XRD) and scanning electron microscopy (SEM) results show that coating the electrode with Nafion during each electrodepositing step plays a crucial role on the morphology, particle size and crystallinity of the electrocatalysts. Although the commercial Pd catalyst has the smaller particle size and more uniform distribution than that prepared by RENC, the RENC electrode exhibits almost the same electrochemical surface area, a better performance and durability toward formic acid electro-oxidation. These results can be attributed to the improved catalyst utilization resulting from the multi-layer structure and the predominance of the highly active Pd (111) crystallite phase on the surface of the catalyst layer.

© 2012 Elsevier B.V. All rights reserved.

1. Introduction

Microfluidic fuel cells, which eliminate the proton exchange membrane and utilize the co-laminar flow nature of multistream in a microfluidic channel to separate the anolyte and the catholyte, are considered as a promising alternative power source for portable devices [1,2]. Microfluidic fuel cells eliminate the membrane-related problems, e.g. membrane degradation and water management, providing an opportunity to develop cost-effective and long-durable energy suppliers. However, their practical applications are hindered by the relatively low power density and poor fuel utilization.

In order to meet the performance requirements for practical applications, the design with a microchannel architecture was usually employed because of its high surface-to-volume ratio. Typically, the planar electrodes, based on carbon paper [3–5], graphite plate [6–14] and metal substrate (e.g. chromium or gold) [15–21] were used in this design. However, the manufacturing costs of these electrodes are relatively high. More importantly, because of the consumption of the electrochemical reaction on the electrode surface, a depletion boundary layer can be formed on the planar electrode and therefore lower the cell performance [14,21,22]. In order to control the depletion boundary layers, a multi-inlet/outlet configuration was proposed [23], but at the expense of the complexity of the whole system. The cell performance can be further enhanced by using porous electrodes, such as carbon paper with a flow-through structure because of the improved mass transfer of reactants [24–27]. However, its practical application was limited by

* Corresponding author. Institute of Engineering Thermophysics, Chongqing University, Chongqing 400030, China. Tel./fax: +86 23 6510 2474.
E-mail address: zhuxun@cqu.edu.cn (X. Zhu).

0378-7753/$ – see front matter © 2012 Elsevier B.V. All rights reserved.
doi:10.1016/j.jpowsour.2012.04.007

the increased pressure drop [28] and the difficulty of depositing catalyst particles inside the micropores.

Recently, the advantage of non-planar electrode has been recognized [29]. E. Kjeang et al. [30] reported a three-dimensional microfluidic fuel cell using an array of cylinder graphite rods as the electrodes. Both better performance and higher fuel utilization than the planar cell were achieved. This result suggests that graphite rods, the low-cost and intrinsic non-planar architectures, are promising electrode substrates for microfluidic fuel cells. In his study, vanadium redox species were used as the fuel and oxidant. However, vanadium is a potential contaminant to the environment [31], and thus should be replaced by the more eco-friendly ones. Formic acid [5,6,8–10,14–17,21,23–25,32–34] is considered as one of the most promising fuels used in microfluidic fuel cells, due to its renewability, high open-circuit potential and facile electro-oxidation on Pd catalyst [35,36]. In order to combine the advantages of the non-planar architecture and using eco-friendly biofuels, the methods for fabricating powerful, highly efficient and low-cost catalyst layer on graphite rods should be taken into account.

Previous studies demonstrated that high performance Pd catalyst layer can be produced by using dip coating [6], spraying [8] or painting the catalyst ink onto the surface of substrate [9,10], sputter deposition and electrodeposition [15,16,24], etc. Among these techniques, electrodeposition of catalyst on the carbon substrate has attracted particular attention due to its ease of preparation, suitability for special-shaped electrode and low-cost requirement. However, the previous study [37] indicated that electrodeposition may induce dendritic growth of catalyst particles and therefore the decreased electrochemical surface area as well as the electrocatalytic performance.

In this paper, an electrodeposition method for preparing the Pd catalyst layer on graphite rods for the anode of microfluidic fuel cells is proposed. This method consists of a repeated procedure involving the electrodeposition of Pd ions onto the graphite rods, followed by Nafion coating (RENC). A series of physicochemical and electrochemical measurements are performed to characterize the performance of the fabricated electrodes. The corresponding results are also compared with other three fabrication methods, including direct electrodeposition (DE), direct electrodeposition with Nafion coating (DENC) and dip coating (DC).

2. Experimental

2.1. Pretreatment of graphite rods

All chemicals were analytical grade and deionized (DI) water was employed throughout. The graphite rod with a diameter of 0.5 mm was used as the substrate. To eliminate the impurities on the surface, the graphite rods were pretreated by the following procedure, i.e.: (i) stirring in 1 M NaOH at 353 K for 30 min, (ii) rinsing with DI water thoroughly, (iii) stirring in 1 M HCl without heating for 3 h to eliminate oxides existed on the surface of graphite rods, (iv) rinsing with DI water thoroughly, and (v) drying in vacuum oven at 353 K.

2.2. Fabrication of Pd catalyst layer on graphite rods

In this study, four methods (direct electrodeposition (DE), direct electrodeposition with Nafion coating (DENC), repeated electrodeposition with Nafion coating (RENC) and dip coating (DC)) were employed to fabricate the electrodes with the same Pd loading (Fig. 1).

DE was performed in an electrochemical cell consisting of a pretreated graphite rod as the working electrode, a spiral platinum wire as the counter electrode and an Ag/AgCl electrode

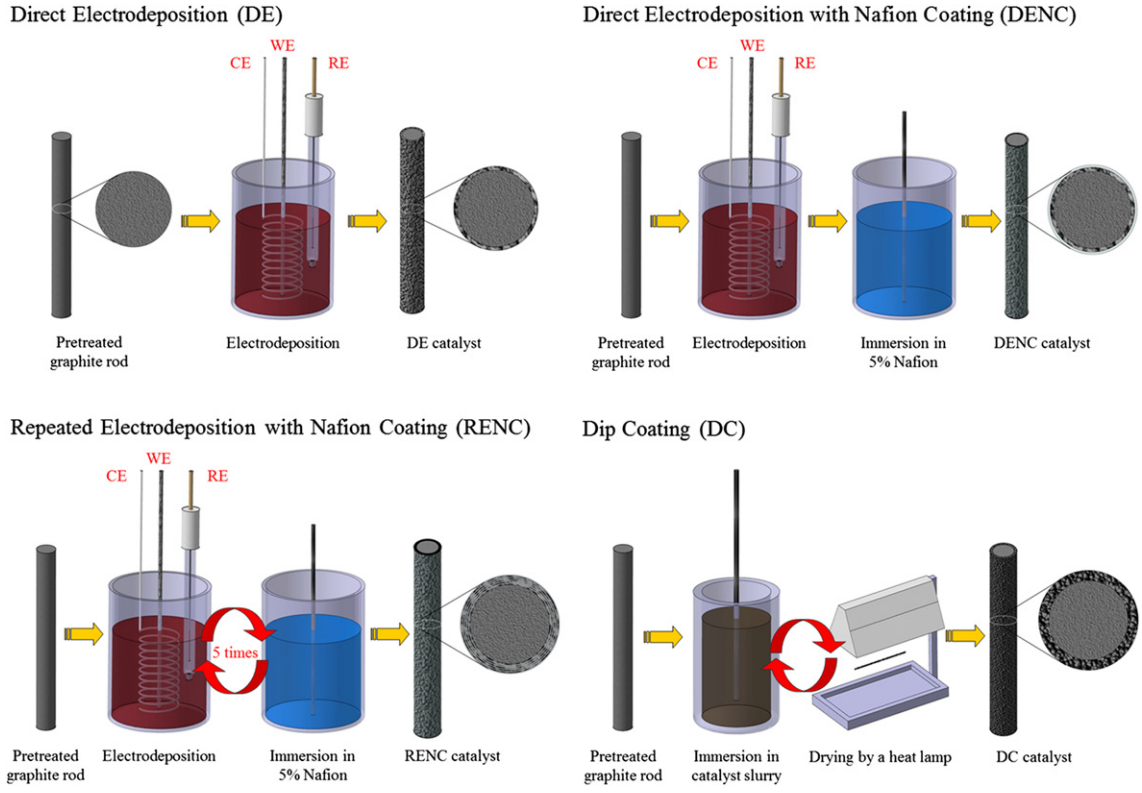

Fig. 1. Schematics of the procedure for fabricating the Pd catalyst layer on graphite rods.

(saturated KCl, 0.198 V vs. SHE) as the reference electrode, respectively. 1.0 wt.% $PdCl_2$ (Sino-Platinum Metals, China) and 1 M HCl in DI water was used as the plating solution [15]. The electrodeposition was performed under potentiostatic control at 0.0 V vs. Ag/AgCl until the desired Pd catalyst loading of 5 mg cm^{-2} was achieved, assuming 60% Coulombic deposition efficiency [15]. DENC is almost the same as DE, except that an extra Nafion layer was coated on the surface of the electrode by repeatedly immersing the electrode into 5 wt.% Nafion® solution (DuPont, USA) and drying in the air. For RENC-prepared electrode, electrodeposition was carried out at the same condition as DE until a Pd loading of 1 mg cm^{-2} was achieved. Then, the electrode was immersed in 5 wt.% Nafion solution for 5 min and dried at room temperature. The amount of added Nafion was determined using an electronic balance (Sartorius CPA225D). The procedure of electrodeposition and Nafion coating was repeated for five times until a Pd loading of 5 mg cm^{-2} was achieved. The Nafion loading of the electrode prepared by RENC was estimated to be 0.3 mg cm^{-2}. This value also determined the target loading of Nafion that should be deposited on the electrode fabricated by DENC.

For DC method, commercial Pd black (Alfa Aesar) was used as the catalyst. Slurry for the catalyst layer was prepared by dispersing Pd black catalyst into a mixture of 5 wt.% Nafion solution and DI water followed by sonicating for 1 h [6]. The composition of catalyst slurry was fixed at Pd black:Nafion (dry weight) = 50:3 to ensure the same Nafion loading (0.3 mg cm^{-2}). The resultant slurry was coated onto the graphite rod by dip coating until the Pd loading achieves 5 mg cm^{-2}. The geometric surface area of the electrodes used in this study was about 0.65 ± 0.02 cm^2.

2.3. Physicochemical characterization

The surface and cross-section morphology of the electrodes fabricated by the four methods were analyzed by using scanning electron microscope (SEM) images, which were obtained by a Tescan Vega II SEM operating at 20 kV. The surfaces of the electrodes were observed without further treatment, while the cross-sections of the electrodes were prepared by breaking the samples after dipping them in liquid nitrogen.

The crystal structure of the catalyst was characterized by powder X-ray diffraction (XRD) using a D/MAX2500PC diffractometer with Cu-Kα radiation ($\lambda = 0.15406$ nm) at room temperature. The 2θ angular regions between 20° and 90° were recorded at a scan rate of 6 mV min^{-1}. The samples of the electrodes fabricated by DE, DENC and RENC were prepared by grinding the Pd catalyst layer together with the graphite rod substrate. The Pd black (Alfa Aesar) was tested as received.

2.4. Electrochemical measurement

All electrochemical measurements were conducted on an electrochemical workstation (Zahner Zennium, Germany) at room temperature. In this study, all the electrochemical measurements were recorded twice to obtain reliable and reproducible results. A conventional three-compartment electrochemical cell was used, comprising a prepared electrode as the working electrode, a spiral platinum wire as the counter electrode and an Ag/AgCl electrode (saturated KCl, 0.198 V vs. SHE) as the reference electrode, respectively. For all electrochemical measurements, the current was normalized to the amount of Pd catalyst loading on the electrodes (mA mg^{-1}) unless stated otherwise. Prior to all electrochemical experiments, high purity nitrogen was fed into the electrolyte for 30 min to eliminate the dissolved oxygen. For the electrochemical experiments, all the potentials were quoted against SHE.

Cyclic voltammetry (CV) experiments were performed in 0.5 M H_2SO_4 with or without 0.5 M HCOOH in the potential range of 0.0 V–0.9 V at a scan rate of 10 mV s^{-1}. Before all experiments, the electrode was cycled for 20 times at a scan rate of 50 mV s^{-1} to obtain a stable voltammogram. The electroactive surface area (ESA) was calculated based on the hydrogen desorption area by assuming 0.21 mC cm^{-2} corresponds to a monolayer of adsorbed hydrogen [38–40]. For CO-stripping experiments, CO was preadsorbed by purging high purity CO gas onto the surface of the electrode in 0.5 M H_2SO_4 solution for 30 min while keeping the electrode potential at 0.1 V [41]. Then the remaining CO in the solution was removed by purging high purity argon for 30 min. Finally, the CO-stripping voltammetry curves are recorded from 0.0 V to 1.2 V at a scan rate of 5 mV s^{-1}.

To evaluate the long-term performance and durability of formic acid electro-oxidation, chronoamperometry (CA) was conducted at 0.34 V in 0.5 M HCOOH + 0.5 M H_2SO_4 for 1800 s. The anodic polarization curves were obtained by stepwise potentiostatic control from open-circuit potential to 0.45 V by 0.05 V increments in 0.5 M HCOOH + 0.5 M H_2SO_4 solution. The corresponding current density of each step was monitored for 3 min to achieve a steady state. The value at the end of each step was used to plot the anodic polarization curves.

3. Results and discussion

3.1. SEM characterization of the electrodes

The typical surface SEM images of the electrodes fabricated by the four methods are shown in Fig. 2 at 5000× magnification. The most notable difference is that the catalysts prepared by DE and DENC (Fig. 2a and b) show a highly developed dendritic structure, while the catalyst prepared by RENC forms an island structure (Fig. 2c). To better understand the different morphologies of the Pd catalysts, the detail structure of the electrodes prepared by DE and RENC are investigated at higher magnification, as shown in the insert views in Fig. 2a and c. The dendritic Pd crystal can be found in Fig. 2a and the dimension of the branch is not uniform, ca. 0.3–1.0 μm along the longitudinal. The dendritic shape of the Pd crystal is known to have deteriorative effects on the catalyst activity because it diminishes the surface area of the catalyst and decreases the performance of the electrode. By contrast, the large Pd islands consist of several Pd aggregates with diameters ranging from 100 nm to 500 nm. It's expected that this structure can extend the electrochemical active surface area, due to the decreased particle size [42,43]. The surface micrograph of the electrode prepared by DC is also present in Fig. 2d. As can be seen, the catalyst surface is rough and porous, and no evident catalyst crystal grain can be seen at 5000× magnification.

The distinct difference in the surface morphology between the electrodes prepared by DE/DENC and RENC implies that the growth mechanisms of the Pd crystal on these electrodes are different. It is known that $PdCl_2$ forms $[PdCl_4]^{2-}$ in HCl solution [44]. For the RENC-prepared electrode, a thin Nafion layer was coated onto the deposited Pd catalyst layer after the first electrodeposition procedure. Due to the electrostatic repulsion between the anionic sulfonic groups in the Nafion layer and $[PdCl_4]^{2-}$ anion in the solution, the concentration of $[PdCl_4]^{2-}$ at the surface of Pd particles formed in the first electrodeposition procedure is lower than that in the bulk. This phenomenon reduces the equilibrium potential ($E_{eq}([PdCl_4]^{2-}/Pd)$), leading to the decrease of the electrodeposition overpotentials ($E_{apply}([PdCl_4]^{2-}/Pd) - E_{eq}([PdCl_4]^{2-}/Pd)$) during the following electrodeposition procedures, as shown in Fig. 3. Here $E_{apply}([PdCl_4]^{2-}/Pd)$ is the applied deposition potential, equal to 0.0 V vs. Ag/AgCl in this study. This reduced

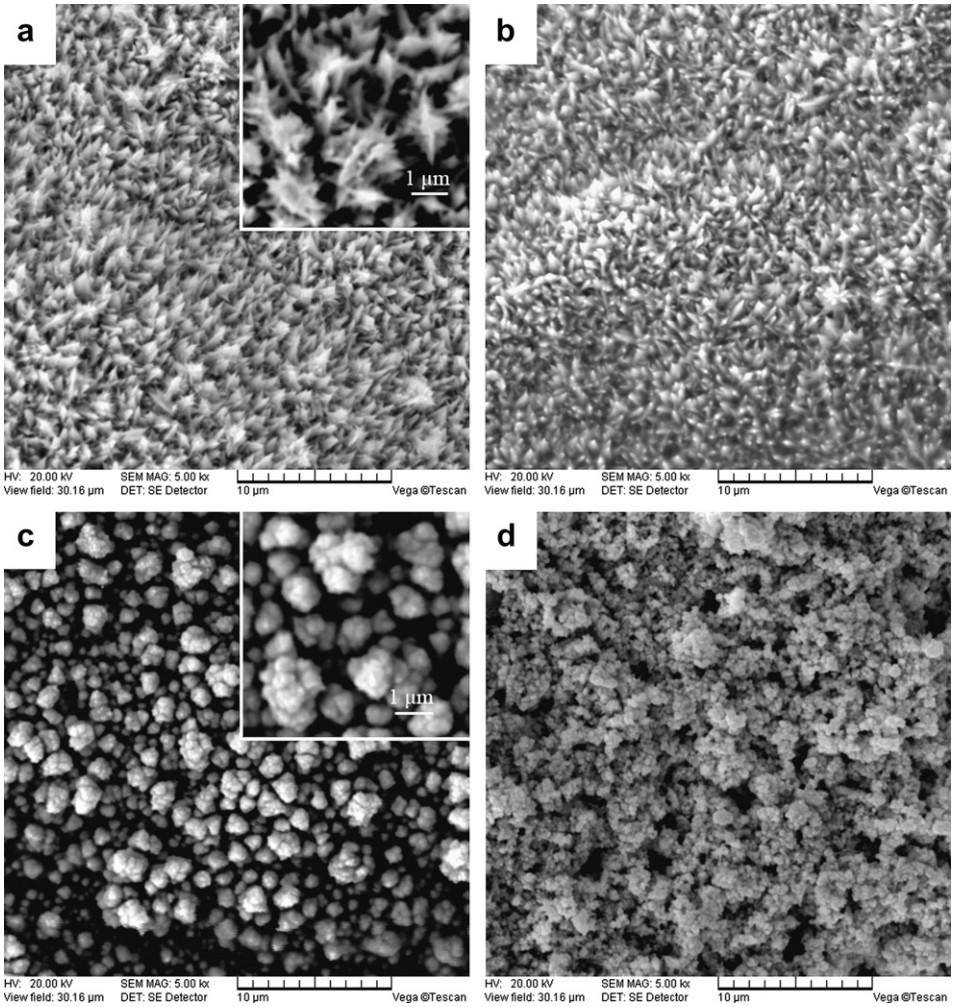

Fig. 2. Surface scanning electron micrographs of the electrodes prepared by (a) DE, (b) DENC, (c) RENC and (d) Pd black, captured at 5000× magnification. Inserts are captured at higher magnification for the surface of Pd catalyst layer prepared by DE and RENC, respectively.

overpotential can decrease the growth rate of the catalyst particles, inducing mixed diffusion/kinetic limited deposition. Under this condition, the radial transport of metal ions in bulk solution results in the formation of hemispherical islands [45]. By contrast, for DE/DENC method, the concentration of $[PdCl_4]^{2-}$ at the electrode surface is similar to that in the bulk, leading to relatively higher deposition overpotentials (see Fig. 3). The resulted fast crystal growth and high flux of metal ions can induce growth instabilities, resulting in the formation of dendritic morphology [46].

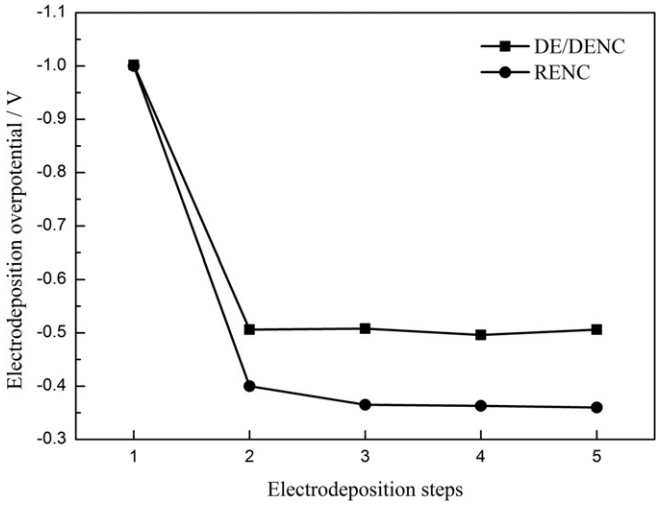

Fig. 3. Electrodeposition overpotentials recorded in the deposition procedure for the electrodes prepared by DE/DENC and RENC.

In this study, the cross-sections of the electrodes are also compared in Fig. 4. From these images, one can find that the electrodes prepared by DE (Fig. 4a) have a similar morphology to that of DENC (Fig. 4b) except for the absence of the Nafion coating on the surface of the electrode. The thickness of the catalyst layer prepared by both methods is about 7 μm. By contract, the catalyst layer prepared by RENC (Fig. 4c) shows a multi-layer structure, and the overall thickness is about 13 μm with the individual layers being between 2 and 4 μm thick. The interconnected interstitial spaces in multi-layer structure may offer the extended three-phase boundary and thus the enhanced Pd utilization. In the case of DC (Fig. 4d), the catalyst layer is about 14 μm, which is slightly thicker than that prepared by RENC because of the more porous structure in the catalyst layer.

3.2. X-ray diffraction (XRD) characterization of the catalysts

Fig. 5 depicts the X-ray diffraction patterns collected from Pd black and powders of the three types. Compared with the Pd black catalyst, additional diffraction peaks located at around 26° and 55°, corresponding to (002) and (004) diffractions of graphitic carbon

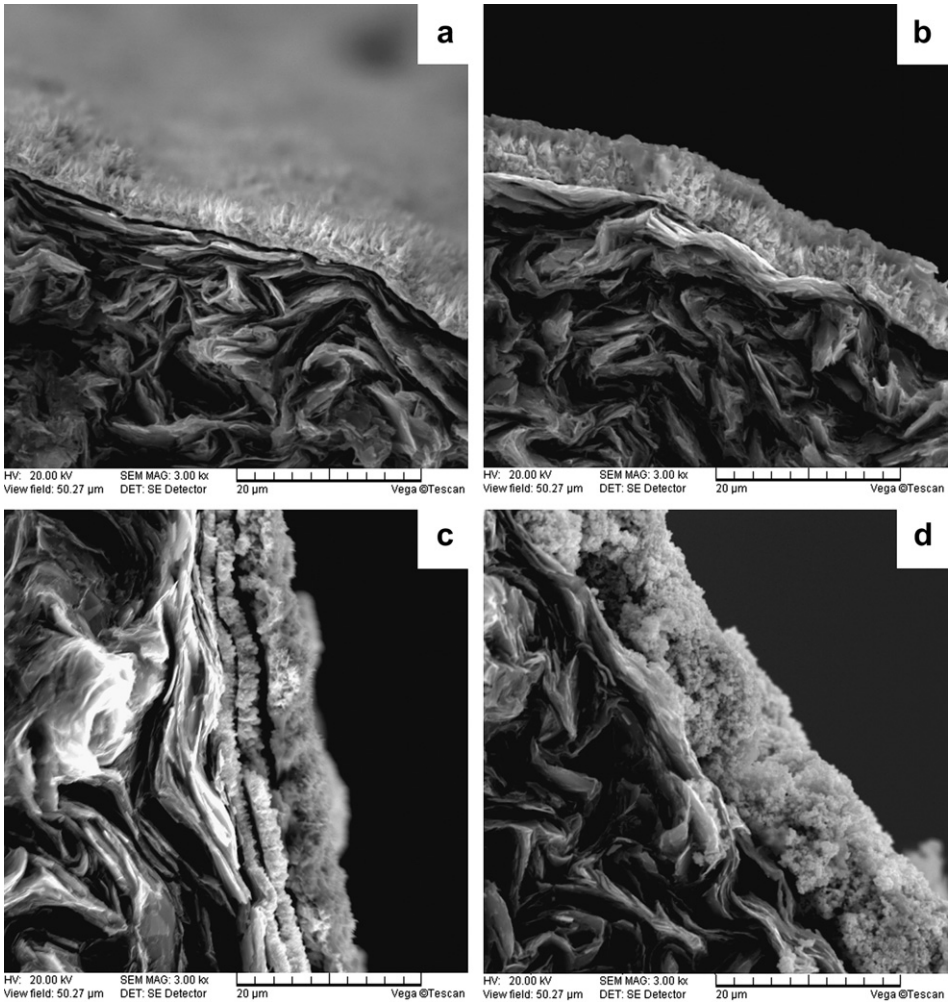

Fig. 4. Cross-section scanning electron micrographs of the electrodes fabricated by (a) DE, (b) DENC, (c) RENC and (d) DC, captured at 3000× magnification.

can be seen for the Pd catalysts fabricated by DE, DENC and RENC. The diffraction peaks at the Bragg angles of 40°, 47°, 68° and 82° correspond to the (111), (200), (220) and (311) facets of Pd crystals respectively. This result indicates that the Pd particles prepared in this study are composed of pure crystalline Pd. Based on the Pd (220) peaks on the patterns, the average sizes of Pd particles are calculated by Debye–Scherrer formula [47] and listed in Table 1:

$$B(2\theta) = 0.94\lambda/L\cos\theta,$$

where $B(2\theta)$ is the half peak width, λ the incident wave-length, L the particle diameter and θ the diffraction angle. As can be found in Table 1, the average particle size of the Pd catalyst fabricated by DE and DENC is 18.3 nm, while the average particle size of the Pd catalysts prepared by RENC and Pd black are estimated to be 17.7 and 17.0 nm, respectively.

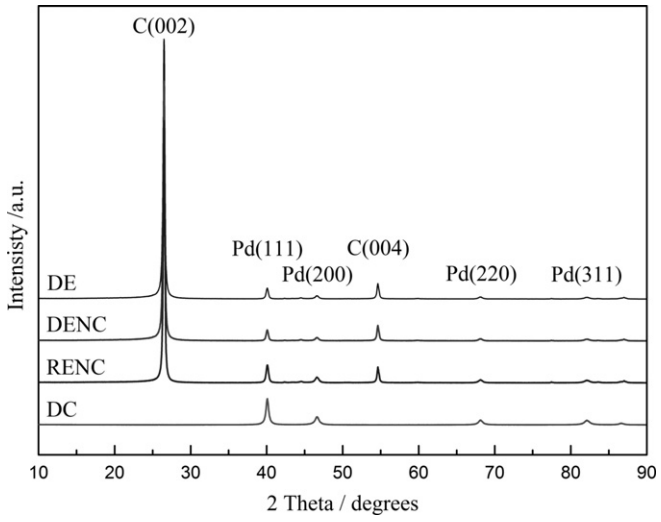

Fig. 5. XRD patterns of the palladium catalysts.

3.3. Cyclic voltammetry (CV)

Fig. 6 illustrates the CV curves recorded for all the electrodes in 0.5 M H_2SO_4 in a potential range from 0.0 V to 0.9 V at a scan rate of

Table 1
Particle sizes, ESA and CO-stripping characteristics for the catalysts.

Electrodes	Particle size (nm)	ESA ($m^2\ g^{-1}$)	Onset potential for CO_{ads} oxidation (V)	Peak potential for CO_{ads} oxidation (V)
DE	18.3	6.75	0.875	0.916
DENC	18.3	7.55	0.873	0.923
RENC	17.7	13.6	0.762	0.831
DC	17.0	14.4	0.825	0.896

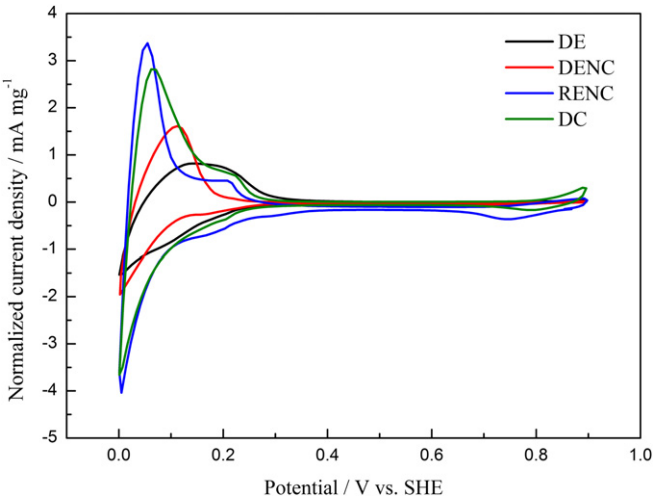

Fig. 6. Cyclic voltammograms of the electrodes in 0.5 M H_2SO_4 at a scan rate of 10 mV s^{-1}.

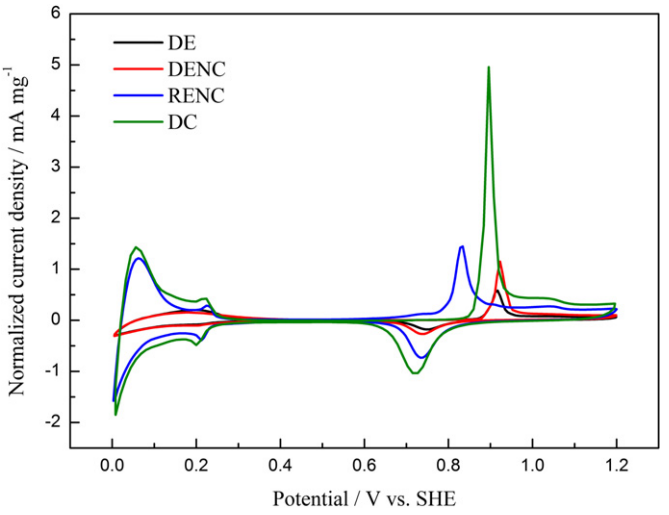

Fig. 7. CO-stripping voltammograms of the electrodes in 0.5 M H_2SO_4 at a scan rate of 5 mV s^{-1}.

10 mV s^{-1}. The electroactive surface area (ESA) is calculated and given in Table 1. The ESA value of the electrode fabricated by DENC is slightly larger than that of DE because of the increased three-phase interface resulting from the existence of the extra Nafion layers. Interestingly, the electrode prepared by RENC exhibits a significantly higher ESA value than those of DE and DENC. This may be attributed to the increased Pd utilization resulting from the extended three-phase boundary between each individual layer (cf. Fig. 4c). In addition, the electrode fabricated by DC has almost the same ESA as that prepared by RENC, which may arise from the smallest catalyst particle size and the porous structure, as discussed before.

It is known that the activity for the formic acid electro-oxidation depends markedly on the crystallographic orientation of Pd [35,48]. In this study, the predominant Pd crystallite planes present on the prepared electrodes are roughly characterized by the hydrogen adsorption/desorption profiles of the CV [49]. As can be seen in Fig. 6, there is a distinct difference in the hydrogen desorption regime between the electrode fabricated by RENC and the other three methods. The CV pattern of this electrode shows a sharp hydrogen desorption peak centered at 0.054 V, followed by a hydrogen desorption shoulder. This unique hydrogen desorption profile can be attributed to the predominance of the Pd (111) crystallite plane in the Pd particles on the surface of the electrode, which is in good agreement with the data reported in the literatures [50–52]. M. Baldauf et al. compared the activity of formic acid electro-oxidation and found that although Pd (110) planes are more active, the Pd (111) planes are more stable and less susceptible to oxidation [53], making (111)-faced Pd catalyst more practical for fuel cell applications [48].

3.4. CO-poison investigation

Fig. 7 displays the typical CO-stripping curves of the four electrodes in 0.5 M H_2SO_4 at 5 mV s^{-1}. The characteristic parameters for CO-stripping experiments are given in Table 1. As presented in Fig. 7 and Table 1, the onset potential of the electrode prepared by RENC for CO_{ads} oxidation is about 0.762 V, almost the same as that on Pd (111) as studied before [52,54]. In the case of the electrodes fabricated by DE, DENC and DC, a positive shift of up to 60 mV for the onset and peak potentials of CO_{ads} oxidation can be observed. From Fig. 7, it is also interesting to find that there is a CO_{ads} oxidation prepeak at 0.569–0.762 V, followed by the main CO-stripping peak centered at 0.831 V. This prepeak arises due to the electro-oxidation of weakly adsorbed CO_{ads}, which can be oxidized at lower overpotentials [55]. The above results imply that the

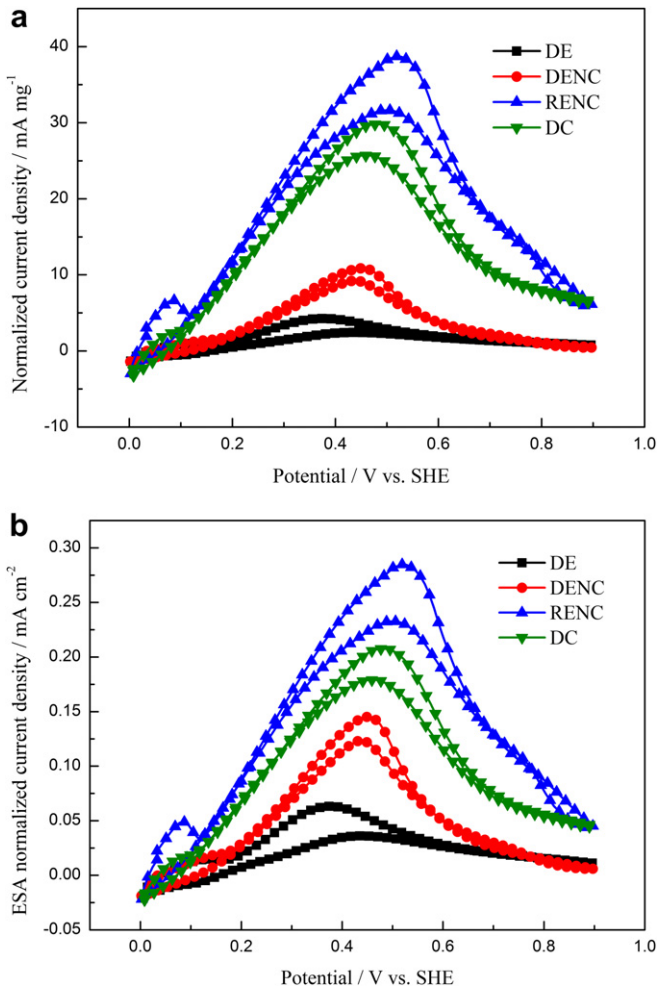

Fig. 8. Mass (a) and electrochemical surface area (b) normalized CV curves of the electrodes in 0.5 M H_2SO_4 + 0.5 M HCOOH at a scan rate of 10 mV s^{-1}.

Table 2
Formic acid electro-oxidation characteristics of the electrodes.

Electrodes	Onset potential (V)	Peak potential (V)	Mass-normalized peak current density (mA mg^{-2})	ESA-normalized peak current density (mA cm^{-2})	Current density at 1800 s (mA mg^{-2})
DE	0.170	0.375	4.3	0.06	0.07
DENC	0.167	0.450	10.9	0.15	0.12
RENC	0.113	0.523	38.6	0.29	6.49
DC	0.108	0.480	29.8	0.21	4.55

electrode prepared by RENC is catalytically more efficient than the other electrodes. This significant difference in the CO_{ads} oxidation kinetics is likely due to the predominant Pd (111) crystal planes present on the RENC-prepared electrode.

3.5. Evaluation of the electrocatalytic activity for formic acid electro-oxidation

To evaluate the electrocatalytic performance of the prepared electrodes, CV curves are recorded in 0.5 M H_2SO_4 + 0.5 M HCOOH in the potential range from 0.0 V to 0.9 V (Fig. 8). The formic acid electro-oxidation current is normalized to the amount of Pd catalyst loading on the electrodes (Fig. 8a). As shown in Fig. 8a, during the reverse potential scan, the anodic current densities arise due to reduction of palladium oxides, exposing fresh Pd atoms sites for the electro-oxidation of formic acid. Furthermore, it can be clearly seen that for the electrode fabricated by DENC, the onset of formic acid electro-oxidation takes place at about 0.167 V (Table 2), almost the same as that prepared by DE. This result suggests that the added Nafion has little effect on the onset potential. As can be seen in Fig. 8a and Table 2, the electrodes fabricated by RENC and DC show an onset potential of more than 50 mV negative than that prepared by DE and DENC. Particularly, for the electrode prepared by RENC, the onset potential is 0.113 V, almost the same as that on Pd (111) as reported in the literature [53]. Results from Fig. 8a demonstrate that the electrocatalytic activity of the electrodes decreases in the following order: RENC > DC > DENC > DE.

In order to evaluate the intrinsic efficiency of the electrodes, the formic acid electro-oxidation current is also normalized to the ESA values and presents in Fig. 8b and Table 2. It can be found that the surface area-specific activities of these electrodes are of the same order as their mass-specific activities. The peak current densities of formic acid electro-oxidation are 0.06, 0.15, 0.29 and 0.21 mA cm^{-2} for the electrodes prepared by DE, DENC, RENC and DC, respectively. From the above results, the RENC-prepared electrode showed the highest activity toward formic acid electro-oxidation. This phenomenon could be attributed to both the increased Pd utilization resulting from the extended three-phase boundary inside the multi-layer structure and the high activity of the predominant Pd (111) on the surface of the catalyst layer. In addition, as mentioned above, several small Pd aggregates on the island could also extend the electrochemical active surface area of the electrode, and therefore has a beneficial effect on the catalytic activity toward formic acid oxidation.

To compare the long-term performance of the electrodes prepared by the four methods, chronoamperometry (CA) measurements are performed in 0.5 M HCOOH + 0.5 M H_2SO_4 with the potentiostatic control at 0.34 V. The chronoamperometry curves are recorded for 1800 s and presented in Fig. 9. The current densities are also normalized to the real surface area of Pd catalysts. For all the electrodes, the curves decrease with time due to the combined effect of the blockage of the electrode surface resulting from the accumulation of CO_2 bubbles [56] and the poisoning effect arising from the formation of intermediates during formic acid electro-oxidation. From Fig. 9, it is obvious that the current density of the electrode prepared by RENC is the highest. At 1800 s, the end of the chronoamperometry measurement, the current density of the electrode fabricated by RENC is 6.49 mA mg^{-2}. This result suggests that the electrode prepared by RENC exhibits the best long-term performance toward the formic acid electro-oxidation.

The anodic polarization curves of the electrodes are also studied in 0.5 M HCOOH + 0.5 M H_2SO_4 and shown in Fig. 10. During the test, the currents are monitored and recorded after 3 min to achieve steady state. As shown in Fig. 10, the current densities of the electrode prepared by RENC are the largest at the potentials higher than 0.15 V. The superior performance of the electrode can be attributed to the increased electrochemical surface area resulting from the mutil-layer structure and the highest electrocatalytic performance

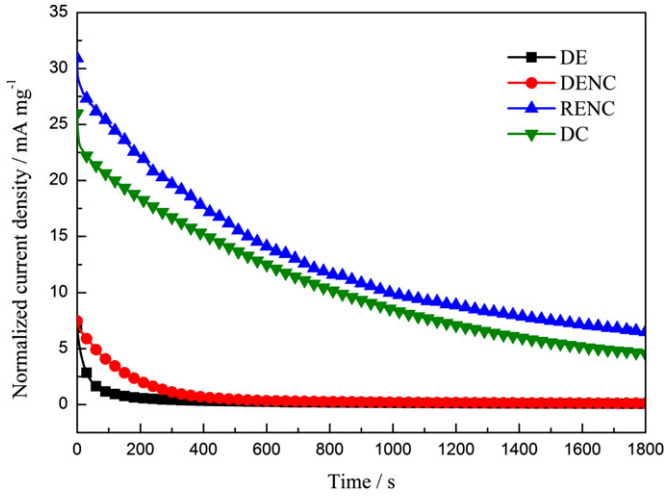

Fig. 9. Chronoamperometry curves of the four electrodes in 0.5 M HCOOH + 0.5 M H_2SO_4 at 0.34 V.

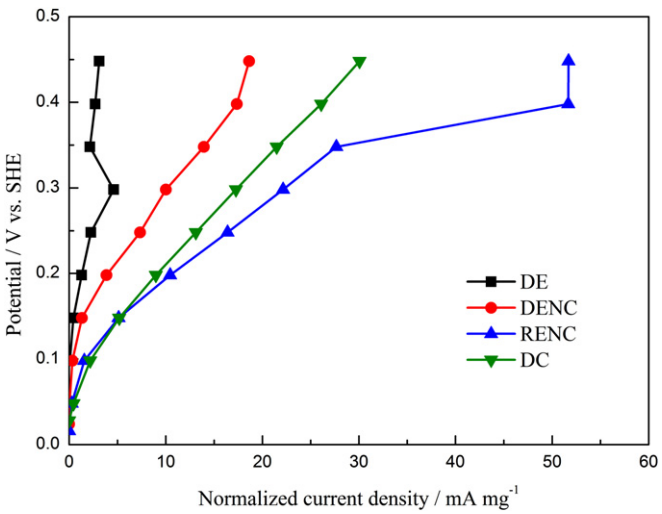

Fig. 10. Anodic polarization curves of the electrodes prepared by the four methods.

for formic acid oxidation, as discussed before. These results confirm that the electrode prepared by the RENC shows a high performance for formic acid electro-oxidation.

4. Conclusion

To take the advantages of the non-planar architecture and eco-friendly biofuels for microfluidic fuel cells, a new method for fabricating non-planar electrodes is proposed and investigated. The results of physicochemical and electrochemical measurements are compared with other three preparation methods including direct electrodeposition (DE), direct electrodeposition with Nafion coating (DENC) and dip coating (DC). The results show that the electrode fabricated by RENC shows a superior performance and durability for the formic acid electro-oxidation to the other three electrodes. It can be attributed to the combined beneficial effects of the increased electrochemical surface area caused by the multi-layer structure and the predominant Pd crystallite planes present on the electrode. The presented method seems to be promising for fabricating non-planar electrodes for microfluidic fuel cells.

Acknowledgments

The authors wish to thank the Natural Science Foundation of China (Grant Nos: 51006130, 51176212), the Natural Science Foundation of Chongqing (Grant No: cstcjjA90009) and the Fundamental Research Funds for the Central Universities (CDJZR11 14 00 01) for the financial support to carry out this study.

References

[1] E. Kjeang, N. Djilali, D. Sinton, J. Power Sources 186 (2009) 353–369.
[2] S.A.M. Shaegh, N.T. Nguyen, S.H. Chan, Int. J. Hydrogen Energy 36 (2011) 5675–5694.
[3] A. Hollinger, R. Maloney, R.S. Jayashree, D. Natarajan, L.J. Markoski, P.J.A. Kenis, J. Power Sources 195 (2010) 3523–3528.
[4] E. Kjeang, B.T. Proctor, A.G. Brolo, D.A. Harrington, N. Djilali, D. Sinton, Electrochim. Acta 52 (2007) 4942–4946.
[5] S.A.M. Shaegh, N. Nam-Trung, C. Siew Hwa, J. Micromech. Microeng. 20 (2010) 105008.
[6] R.S. Jayashree, L. Gancs, E.R. Choban, A. Primak, D. Natarajan, L.J. Markoski, P.J.A. Kenis, J. Am. Chem. Soc. 127 (2005) 16758–16759.
[7] R.S. Jayashree, D. Egas, J.S. Spendelow, D. Natarajan, L.J. Markoski, P.J.A. Kenis, Electrochem. Solid-State Lett. 9 (2006) A252–A256.
[8] A.S. Gago, D. Morales-Acosta, L.G. Arriaga, N. Alonso-Vante, J. Power Sources 196 (2011) 1324–1328.
[9] F.R. Brushett, R.S. Jayashree, W.P. Zhou, P.J.A. Kenis, Electrochim. Acta 54 (2009) 7099–7105.
[10] R.S. Jayashree, S.K. Yoon, F.R. Brushett, P.O. Lopez-Montesinos, D. Natarajan, L.J. Markoski, P.J.A. Kenis, J. Power Sources 195 (2010) 3569–3578.
[11] E.R. Choban, J. Spendelow, L. Gancs, A. Wieckowski, P. Kenis, Electrochim. Acta 50 (2005) 5390–5398.
[12] J.-C. Shyu, C.-L. Huang, J. Power Sources 196 (2011) 3233–3238.
[13] E.R. Choban, P. Waszczuk, P.J.A. Kenis, Electrochem. Solid-State Lett. 8 (2005) A348–A352.
[14] F.R. Brushett, A.S. Hollinger, L.J. Markoski, P.J.A. Kenis, ASME Conference Proceedings 2009, 2009, pp. 247–252.
[15] E. Kjeang, A.G. Brolo, D.A. Harrington, N. Djilali, D. Sinton, J. Electrochem. Soc. 154 (2007) B1220–B1226.
[16] P.O. López-Montesinos, N. Yossakda, A. Schmidt, F.R. Brushett, W.E. Pelton, P.J.A. Kenis, J. Power Sources 196 (2011) 4638–4645.
[17] M. Sun, G. Velve Casquillas, S. Guo, J. Shi, H. Ji, Q. Ouyang, Y. Chen, Microelectron. Eng. 84 (2007) 1182–1185.
[18] I.B. Sprague, P. Dutta, S. Ha, Proc. IMechE Part A: J. Power and Energy 223 (2009) 799–808.
[19] I.B. Sprague, P. Dutta, S. Ha, ASME Conference Proceedings 2008, 2008, pp. 885–889.
[20] R. Ferrigno, A.D. Stroock, T.D. Clark, M. Mayer, G.M. Whitesides, J. Am. Chem. Soc. 124 (2002) 12930–12931.
[21] E.R. Choban, L.J. Markoski, A. Wieckowski, P.J.A. Kenis, J. Power Sources 128 (2004) 54–60.
[22] A. Zebda, L. Renaud, M. Cretin, C. Innocent, F. Pichot, R. Ferrigno, S. Tingry, J. Power Sources 193 (2009) 602–606.
[23] S.K. Yoon, G.W. Fichtl, P.J.A. Kenis, Lab. Chip 6 (2006) 1516–1524.
[24] E. Kjeang, R. Michel, D.A. Harrington, D. Sinton, N. Djilali, Electrochim. Acta 54 (2008) 698–705.
[25] K.S. Salloum, J.R. Hayes, C.A. Friesen, J.D. Posner, J. Power Sources 180 (2008) 243–252.
[26] J.R. Hayes, A.M. Engstrom, C. Friesen, J. Power Sources 183 (2008) 257–259.
[27] K.S. Salloum, J.D. Posner, J. Power Sources 196 (2011) 1229–1234.
[28] E. Kjeang, R. Michel, D.A. Harrington, N. Djilali, D. Sinton, J. Am. Chem. Soc. 130 (2008) 4000–4006.
[29] W.R. Merida, G. McLean, N. Djilali, J. Power Sources 102 (2001) 178–185.
[30] E. Kjeang, J. McKechnie, D. Sinton, N. Djilali, J. Power Sources 168 (2007) 379–390.
[31] S.M. Glenn, L. James Lester, J. Hydrol. 389 (2010) 214–226.
[32] J.L. Cohen, D.A. Westly, A. Pechenik, H.D. Abruna, J. Power Sources 139 (2005) 96–105.
[33] A. Li, S.H. Chan, N.T. Nguyen, J. Micromech. Microeng. 17 (2007) 1107.
[34] D. Morales-Acosta, G. Rodriguez, J. Power Sources 195 (2010) 1862–1865.
[35] W. Zhou, J.Y. Lee, J. Phys. Chem. C 112 (2008) 3789–3793.
[36] R.D. Morgan, A. Salehi-Khojin, R.I. Masel, J. Phys. Chem. C 115 (2011) 19413–19418.
[37] H. Kim, N.P. Subramanian, B.N. Popov, J. Power Sources 138 (2004) 14–24.
[38] J. Ge, X. Chen, C. Liu, T. Lu, J. Liao, L. Liang, W. Xing, Electrochim. Acta 55 (2010) 9132–9136.
[39] C.-T. Hsieh, Y.-Y. Liu, Y.-S. Cheng, W.-Y. Chen, Electrochim. Acta 56 (2011) 6336–6344.
[40] X. Huang, S. Tang, X. Mu, Y. Dai, G. Chen, Z. Zhou, F. Ruan, Z. Yang, N. Zheng, Nat. Nano. 6 (2011) 28–32.
[41] J. Solla-Gullon, A. Rodes, V. Montiel, A. Aldaz, J. Clavilier, J. Electroanal. Chem. 554 (2003) 273–284.
[42] Y.-L. Wang, Y.-Q. Zhao, C.-L. Xu, D.-D. Zhao, M.-W. Xu, Z.-X. Su, H.-L. Li, J. Power Sources 195 (2010) 6496–6499.
[43] W. Yang, S. Yang, W. Sun, G. Sun, Q. Xin, Electrochim. Acta 52 (2006) 9–14.
[44] H.A. Droll, B. Block, W.C. Fernelius, J. Phys. Chem. 61 (1957) 1000–1004.
[45] G. Lian, O. Gerko, R. Aleksandar, M.H. Peter, C.S. Peter, J. Phys. D: Appl. Phys. 44 (2011) 443001.
[46] L. Guo, P.C. Searson, Electrochim. Acta 55 (2010) 4086–4091.
[47] L. Zhang, T. Lu, J. Bao, Y. Tang, C. Li, Electrochem. Commun. 8 (2006) 1625–1627.
[48] V. Mazumder, S. Sun, J. Am. Chem. Soc. 131 (2009) 4588–4589.
[49] J. Prabhuram, T. Zhao, Z. Tang, R. Chen, Z. Liang, J. Phys. Chem. B 110 (2006) 5245–5252.
[50] N. Hoshi, K. Kida, M. Nakamura, M. Nakada, K. Osada, J. Phys. Chem. B 110 (2006) 12480–12484.
[51] A.M. El-Aziz, L.A. Kibler, D.M. Kolb, Electrochem. Commun. 4 (2002) 535–539.
[52] A.M. El-Aziz, L.A. Kibler, J. Electroanal. Chem. 534 (2002) 107–114.
[53] M. Baldauf, D.M. Kolb, J. Phys. Chem. 100 (1996) 11375–11381.
[54] S. Zou, R. Gómez, M.J. Weaver, J. Electroanal. Chem. 474 (1999) 155–166.
[55] N.M. Marković, B.N. Grgur, C.A. Lucas, P.N. Ross, J. Phys. Chem. B 103 (1999) 487–495.
[56] P. Babu, H. Kim, J. Chung, E. Oldfield, A. Wieckowski, J. Phys. Chem. B 108 (2004) 20228–20232.